Nonlinear Dyn
DOI 10.1007/s11071-009-9636-3

REVIEW PAPER

Nonlinear complexity of human biodynamics engine

Vladimir G. Ivancevic

Received: 23 July 2009 / Accepted: 2 December 2009

Abstract This paper reviews a nonlinear complexity within the Human Biodynamics Engine (HBE), a world-class human neuro-musculoskeletal simulator, developed at the Department of Defense, Australia. The HBE development is based on an anthropomorphic tree of Euclidean motion groups $SE(3)$, with 270 active degrees of freedom, realistic muscular mechanics and hierarchical neural-like control. The HBE is formulated in the fashion of nonlinear dynamics/control of highly complex biophysical and robotic systems and developed for the purpose of neuro-musculoskeletal injury prediction. The following aspects of the HBE development are described: geometrical, dynamical, control, physiological, biomedical, AI, behavioral and complexity. Several simulation examples are provided.

Keywords Human biodynamics engine · Tree of Euclidean motion groups $SE(3)$ · Lagrangian/Hamiltonian biodynamics · Hierarchical nonlinear control · Neuromuscular mechanics · Fuzzy-topological coordination · Injury prediction

V.G. Ivancevic (✉)
Land Operations Division, Defense Science & Technology Organisation, P.O. Box 1500, Edinburgh, SA 5111, Australia
e-mail: Vladimir.Ivancevic@dsto.defence.gov.au

1 Introduction

Both human biodynamics and humanoid robotics are devoted to studying human-like motion. They are both governed by Newtonian dynamical laws and reflex-like nonlinear controls [1–8].

Although current humanoid robots more and more resemble human motion, we still need to emphasize that human joints are (and will probably always remain) significantly more flexible than humanoid robot joints. Namely, each humanoid joint consists of a pair of coupled segments with only Eulerian rotational degrees of freedom. On the other hand, in each human synovial joint, besides gross Eulerian rotational movements (roll, pitch and yaw), we also have some hidden and restricted translations along (X, Y, Z)-axes. For example, in the knee joint, patella (knee cap) moves for about 7–10 cm from maximal extension to maximal flexion. It is well known that even greater are translational amplitudes in the shoulder joint. In other words, within the realm of rigid body mechanics, a segment of a human arm or leg is not properly represented as a rigid body fixed at a certain point, but rather as a rigid body hanging on rope-like ligaments. More generally, the whole skeleton mechanically represents a system of flexibly coupled rigid bodies, technically an anthropomorphic topological product of $SE(3)$-groups. This implies the more complex kinematics, dynamics and control than in the case of humanoid robots [9].

Published online: 07 January 2010

This paper presents the scientific body of knowledge behind the sophisticated human motion simulator, formulated in the fashion of nonlinear humanoid robotics, called the Human Biodynamics Engine (HBE), designed over the last five years by the present author at Defense Science & Technology Organisation, Australia. The HBE is a sophisticated human neuro-musculoskeletal dynamics simulator, based on generalized Lagrangian and Hamiltonian mechanics and Lie-derivative nonlinear control. It includes 270 active degrees of freedom (DOF), without fingers: 135 rotational DOF are considered active, and 135 translational DOF are considered passive. The HBE incorporates both forward and inverse dynamics, as well as two neural-like control levels. Active rotational joint dynamics is driven by 270 nonlinear muscular actuators, each with its own excitation/contraction dynamics (following traditional Hill–Hatze biomechanical models). Passive translational joint dynamics models viscoelastic properties of intervertebral discs, joint tendons and muscular ligaments as a nonlinear spring–damper system. The lower neural control level resembles spinal-reflex positive and negative force feedbacks, resembling stretch and Golgi reflexes, respectively. The higher neural control level mimics cerebellum postural stabilization and velocity target-tracking control. The HBE's core is the full spine simulator, considering human spine as a chain of 26 flexibly-coupled rigid bodies (formally, the product of 26 $SE(3)$-groups). The HBE includes over 3000 body parameters, all derived from individual user data, using standard biomechanical tables. The HBE incorporates a new theory of soft neuro-musculoskeletal injuries, based on the concept of the local rotational and translational jolts, which are the time rates of change of the total forces and torques localized in each joint at a particular time instant.

2 Geometrical formalism of human–robot biodynamics

2.1 Configuration manifold of idealistic robot motion

Representation of an ideal humanoid–robot motion is rigorously defined in terms of rotational constrained $SO(3)$-groups [6, 8, 10, 11] in all main robot joints (see Fig. 1). Therefore, the configuration manifold Q_{rob} for humanoid dynamics is defined as a topological product of all included $SO(3)$-groups, $Q_{\text{rob}} = \prod_i SO(3)^i$. Consequently, the natural stage for autonomous Lagrangian dynamics of robot motion is the tangent bundle TQ_{rob}[1] [5], and for the corresponding autonomous Hamiltonian dynamics is the cotangent bundle T^*Q_{rob}[2] [2, 3].

More precisely, the three-axial $SO(3)$-group of humanoid–robot joint rotations depends on three parameters, Euler joint angles $q^i = (\varphi, \psi, \theta)$, defining the rotations about the Cartesian coordinate triedar (x, y, z) placed at the joint pivot point. Each of the Euler angles is defined in the constrained range $(-\pi, \pi)$, so the joint group space is a constrained sphere of radius π [6, 8, 10].

Let $G = SO(3) = \{A \in \mathcal{M}_{3\times 3}(\mathbb{R}) : A^t A = I_3, \det(A) = 1\}$ be the group of rotations in $\mathbb{R}^3$. It is a Lie group and $\dim(G) = 3$. Let us isolate its one-parameter joint subgroups, i.e., consider the three operators of the finite joint rotations $R_\varphi, R_\psi, R_\theta \in SO(3)$, given by

$$R_\varphi = \begin{bmatrix} 1 & 0 & 0 \\ 0 & \cos\varphi & -\sin\varphi \\ 0 & \sin\varphi & \cos\varphi \end{bmatrix},$$

[1] In mechanics, to each n-dimensional (nD) configuration manifold Q there is its associated $2n$D velocity phase-space manifold, denoted by TM and called the tangent bundle of Q. The original smooth manifold Q is called the base of TM. There is an onto map $\pi : TM \to Q$, called the projection. Above each point $x \in Q$ there is a tangent space $T_xQ = \pi^{-1}(x)$ to Q at x, which is called a fiber. The fiber $T_xQ \subset TM$ is the subset of TM, such that the total tangent bundle, $TM = \coprod_{m\in Q} T_xQ$, is a disjoint union of tangent spaces T_xQ to Q for all points $x \in Q$. From dynamical perspective, the most important quantity in the tangent bundle concept is the smooth map $v : Q \to TM$, which is an inverse to the projection π, i.e., $\pi \circ v = \text{Id}_Q$, $\pi(v(x)) = x$. It is called the velocity vector-field. Its graph $(x, v(x))$ represents the cross section of the tangent bundle TM. This explains the dynamical term velocity phase-space, given to the tangent bundle TM of the manifold Q. The tangent bundle is where tangent vectors live, and is itself a smooth manifold. Vector-fields are cross sections of the tangent bundle.

System's Lagrangian (energy function) is a natural energy function on the tangent bundle.

[2] A dual notion to the tangent space T_mQ to a smooth manifold Q at a point m is its cotangent space T_m^*Q at the same point m. Similarly to the tangent bundle, for a smooth manifold Q of dimension n, its cotangent bundle T^*Q is the disjoint union of all its cotangent spaces T_m^*Q at all points $m \in Q$, i.e., $T^*Q = \coprod_{m\in Q} T_m^*Q$. Therefore, the cotangent bundle of an n-manifold Q is the vector bundle $T^*Q = (TM)^*$, the (real) dual of the tangent bundle TM. The cotangent bundle is where 1-forms live, and is itself a smooth manifold. Co-vector fields (1-forms) are cross sections of the cotangent bundle. The Hamiltonian is a natural energy function on the tangent bundle.

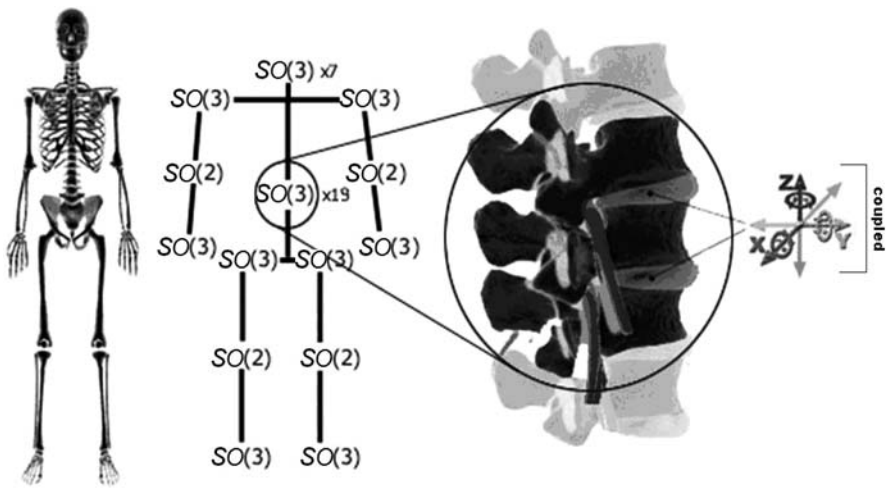

Fig. 1 The configuration manifold Q_{rob} of the humanoid–robot body is defined as a topological product of constrained $SO(3)$-groups, $Q_{\text{rob}} = \prod_i SO(3)^i$

$$R_\psi = \begin{bmatrix} \cos\psi & 0 & \sin\psi \\ 0 & 1 & 0 \\ -\sin\psi & 0 & \cos\psi \end{bmatrix},$$

$$R_\theta = \begin{bmatrix} \cos\theta & -\sin\theta & 0 \\ \sin\theta & \cos\theta & 0 \\ 0 & 0 & 1 \end{bmatrix}$$

corresponding respectively to rotations about x-axis by an angle φ, about y-axis by an angle ψ, and about z-axis by an angle θ.

The total three-axial joint rotation A is defined as the product of the above one-parameter rotations R_φ, R_ψ, R_θ, i.e., $A = R_\varphi \cdot R_\psi \cdot R_\theta$ is equal to[3]

$$A = \begin{bmatrix} \cos\psi\cos\varphi - \cos\theta\sin\varphi\sin\psi & \cos\psi\cos\varphi + \cos\theta\cos\varphi\sin\psi & \sin\theta\sin\psi \\ -\sin\psi\cos\varphi - \cos\theta\sin\varphi\sin\psi & -\sin\psi\sin\varphi + \cos\theta\cos\varphi\cos\psi & \sin\theta\cos\psi \\ \sin\theta\sin\varphi & -\sin\theta\cos\varphi & \cos\theta \end{bmatrix}.$$

However, the order of these matrix products matters: different order products give different results, as the matrix product is noncommutative product. This is the reason why Hamilton's quaternions[4] are today commonly used to parameterize the $SO(3)$-group, especially in the field of 3D computer graphics.

The one-parameter rotations $R_\varphi, R_\psi, R_\theta$ define curves in $SO(3)$ starting from

$$I_3 = \begin{pmatrix} 1 & 0 & 0 \\ 0 & 1 & 0 \\ 0 & 0 & 1 \end{pmatrix}.$$

Their derivatives in $\varphi = 0$, $\psi = 0$ and $\theta = 0$, belong to the associated tangent Lie algebra $\mathfrak{so}(3)$. That is, the corresponding infinitesimal generators of joint rotations—joint angular velocities $v_\varphi, v_\psi, v_\theta \in \mathfrak{so}(3)$—are respectively given by

$$v_\varphi = \begin{bmatrix} 0 & 0 & 0 \\ 0 & 0 & -1 \\ 0 & 1 & 0 \end{bmatrix} = -y\frac{\partial}{\partial z} + z\frac{\partial}{\partial y},$$

[3] Note that this product is noncommutative, so it really depends on the order of multiplications.

[4] Recall that the set of Hamilton's quaternions $\mathbb{H}$ represents an extension of the set of complex numbers $\mathbb{C}$. We can compute a rotation about the unit vector, $\mathbf{u}$, by an angle θ. The quaternion q that computes this rotation is

$$q = \left(\cos\frac{\theta}{2}, u\sin\frac{\theta}{2}\right).$$

$$v_\psi = \begin{bmatrix} 0 & 0 & 1 \\ 0 & 0 & 0 \\ -1 & 0 & 0 \end{bmatrix} = -z\frac{\partial}{\partial x} + x\frac{\partial}{\partial z},$$

$$v_\theta = \begin{bmatrix} 0 & -1 & 0 \\ 1 & 1 & 0 \\ 0 & 0 & 0 \end{bmatrix} = -x\frac{\partial}{\partial y} + y\frac{\partial}{\partial x}.$$

Moreover, the elements are linearly independent and so

$$\mathfrak{so}(3) = \left\{ \begin{bmatrix} 0 & -a & b \\ a & 0 & -\gamma \\ -b & \gamma & 0 \end{bmatrix} \middle| \, a, b, \gamma \in \mathbb{R} \right\}.$$

The Lie algebra $\mathfrak{so}(3)$ is identified with $\mathbb{R}^3$ by associating to each $v = (v_\varphi, v_\psi, v_\theta) \in \mathbb{R}^3$ the matrix $v \in \mathfrak{so}(3)$ given by

$$v = \begin{bmatrix} 0 & -a & b \\ a & 0 & -\gamma \\ -b & \gamma & 0 \end{bmatrix}.$$

Then we have the following identities:

1. $\widehat{u \times v} = [\hat{u}, v]$; and
2. $u \cdot v = -\frac{1}{2}\,\mathrm{Tr}(\hat{u} \cdot v)$.

The exponential map $\exp : \mathfrak{so}(3) \to SO(3)$ is given by Rodrigues relation

$$\exp(v) = I + \frac{\sin\|v\|}{\|v\|}v + \frac{1}{2}\left(\frac{\sin\frac{\|v\|}{2}}{\frac{\|v\|}{2}}\right)^2 v^2,$$

where the norm $\|v\|$ is given by

$$\|v\| = \sqrt{\left(v^1\right)^2 + \left(v^2\right)^2 + \left(v^3\right)^2}.$$

The dual, cotangent Lie algebra $\mathfrak{so}(3)^*$ includes the three-joint angular momenta $p_\varphi, p_\psi, p_\theta \in \mathfrak{so}(3)^*$, derived from the joint velocities v by multiplying them with corresponding moments of inertia.

2.2 Configuration manifold of realistic human motion

On the other hand, human joints are more flexible than robot joints [9]. Namely, every rotation in all synovial human joints is followed by the corresponding micro-translation, which occurs after the rotational amplitude is reached [11]. So, representation of human motion is rigorously defined in terms of Euclidean $SE(3)$-groups of full rigid-body motion [6, 8, 10, 12] in all main human joints (see Fig. 2). Therefore, the configuration manifold Q_{hum} for human dynamics is defined as a topological product of all included constrained $SE(3)$-groups, $Q_{\mathrm{rob}} = \prod_i SE(3)^i$. Consequently, the natural stage for autonomous Lagrangian dynamics of human motion is the tangent bundle TQ_{hum} [5], and for the corresponding autonomous Hamiltonian dynamics is the cotangent bundle T^*Q_{hum} [2–4].

Briefly, the special Euclidean $SE(3)$-group is defined as a semidirect (noncommutative) product of 3D rotations and 3D translations, $SE(3) := SO(3) \triangleright \mathbb{R}^3$. $SE(3)$ is the Lie group consisting of isometries of the Euclidean 3D space $\mathbb{R}^3$ (see [8, 10, 13], for technical details). Its most important subgroups are given in Table 1.

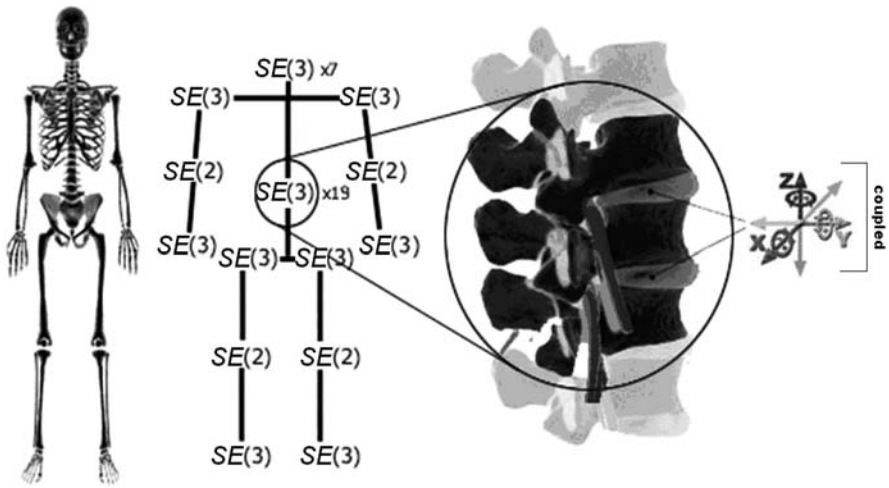

Fig. 2 The configuration manifold Q_{hum} of the human body is defined as a topological product of constrained $SE(3)$-groups acting in all major (synovial) human joints, $Q_{\mathrm{hum}} = \prod_i SE(3)^i$

Table 1

Subgroup	Definition
$SO(3)$, group of rotations in 3D (a spherical joint)	Set of all proper orthogonal 3×3 rotational matrices
$SE(2)$, special Euclidean group in 2D (all planar motions)	Set of all 3×3-matrices: $\begin{bmatrix} \cos\theta & \sin\theta & r_x \\ -\sin\theta & \cos\theta & r_y \\ 0 & 0 & 1 \end{bmatrix}$
$SO(2)$, group of rotations in 2D subgroup of $SE(2)$-group (a revolute joint)	Set of all proper orthogonal 2×2 rotational matrices included in $SE(2)$-group
$\mathbb{R}^3$, group of translations in 3D (all spatial displacements)	Euclidean 3D vector space

2.3 The covariant force law and mechanics of musculoskeletal injury

The $SE(3)$-dynamics applied to human body gives the fundamental law of biomechanics, which is the *Covariant Force Law* [6–8, 10]. It states:

Force co-vector field

= Mass distribution × Acceleration vector field,

which is formally written (using Einstein's summation convention over repeating indices, with indices labeling the three Cartesian (X–Y–Z)-translations and the corresponding three Euler angles) as:

$$F_\mu = m_{\mu\nu} a^\nu \quad (\mu, \nu = 1, \ldots, 6),$$

where F_μ denotes the six covariant components of the external "pushing" $SE(3)$-force co-vector field, $m_{\mu\nu}$ represents the 6×6 covariant components of proximal segment's inertia-metric tensor, while a^ν corresponds to the six contravariant components of the segment's internal $SE(3)$-acceleration vector-field. This law states that contrary to common perception, acceleration and force are not quantities of the same nature: while acceleration is a noninertial vector field, force is an inertial co-vector field. This apparently insignificant difference becomes crucial in injury prediction/prevention, as formalized below. Geometrical elaboration of the covariant force law (briefly shown in Fig. 3) is fully elaborated in [6–8, 10].

Now we come to injury prediction. It was shown in [6, 7] that the general cause of spinal and other musculoskeletal injuries is the $SE(3)$-jolt, which is a sharp

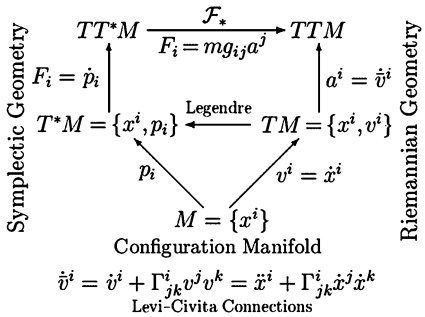

Fig. 3 Riemannian-symplectic geometry of the *Covariant Force Law*

and sudden change in the $SE(3)$-force acting on the mass–inertia distribution of the proximal segment to the injured joint. The $SE(3)$-jolt is a 'delta'-change in a total 3D force-vector acting on joint coupled to a total 3D torque-vector. In other words, the $SE(3)$-jolt is a sudden, sharp and discontinued shock in all six coupled DOF, distributed along the three Cartesian (x, y, z)-translations and the three corresponding Euler angles around the Cartesian axes: roll, pitch and yaw. The $SE(3)$-jolt is rigorously defined in terms of differential geometry [8, 10]. Briefly, it is the absolute time-derivative of the covariant force 1-form acting on the joint.

Formally, the covariant (absolute, Bianchi) time-derivative $\frac{D}{dt}(\cdot)$ of the covariant $SE(3)$-force F_μ defines the corresponding external "striking" $SE(3)$-jolt co-vector field

$$\frac{D}{dt}(F_\mu) = m_{\mu\nu} \frac{D}{dt}\left(a^\nu\right) = m_{\mu\nu}\left(\dot{a}^\nu + \Gamma^\nu_{\mu\lambda} a^\mu a^\lambda\right), \qquad (1)$$

where $\frac{D}{dt}(a^\nu)$ denotes the six contravariant components of the proximal segment's internal $SE(3)$-jerk vector-field and overdot $(\dot{})$ denotes the time derivative. $\Gamma^\nu_{\mu\lambda}$ are the Christoffel's symbols of the Levi-Civita connection for the $SE(3)$-group, which are zero in case of pure Cartesian translations and nonzero in case of rotations as well as in the full-coupling of translations and rotations.

In particular, the spine, or vertebral column, dynamically represents a chain of 26 movable vertebral bodies, joint together by transversal viscoelastic intervertebral discs and longitudinal elastic tendons (see Fig. 4). Textbooks on functional anatomy describe the following spinal movements: (a) cervical intervertebral joints allow all three types of movements: flexion and extension (in the sagittal plane),

Fig. 4 Reference frame of the Human Biodynamics Engine (HBE). The purpose of the HBE simulator is prediction of the risk of soft spinal and other musculoskeletal injuries, as well as biodynamical behavior modeling

lateral flexion (in the frontal plane) and rotation (in the transverse plane); (b) thoracic joints allow rotation and lateral flexion (limited by ribs), while flexion/extension is prevented; and (c) lumbar joints allow flexion/extension as well as limited lateral flexion, while rotation is prevented. This popular picture is fine for the description of safe spinal movements; however, to be able to predict and prevent spinal injuries (both soft ones related to the back-pain syndrome and hard ones related to discus hernia), which are in the domain of unsafe intervertebral movements, a much more rigorous description is needed. The main cause of spinal injuries is the $SE(3)$-jolt, a shock that breaks the spinal structure and/or function.

2.4 Lagrangian formulation of biodynamics

The general form of Lagrangian human/humanoid biodynamics on the corresponding Riemannian tangent bundles $TQ_{\rm rob}$ and $TQ_{\rm hum}$ of the configuration manifolds $Q_{\rm rob}$ and $Q_{\rm hum}$ (precisely derived in [5, 6, 8]) can be formulated in a unified form as:

$$\frac{d}{dt}L_{\dot{x}^i} - L_{x^i} = \mathcal{F}_i(t, x, \dot{x}) \quad (i = 1, \ldots, n) \tag{2}$$

where n denotes the number of DOF for both $n_{\rm hum}$ and $n_{\rm rob}$, $L = L(t, x, \dot{x}) : TQ \to \mathbb{R}$ is the human/humanoid Lagrangian function, defined on the $(2n + 1)$-dimensional jet manifolds,[5] $X_{\rm rob} = J^1_{\rm rob}(\mathbb{R}, Q_{\rm rob}) \cong \mathbb{R} \times TQ_{\rm rob}$ and $X_{\rm hum} = J^1_{\rm hum}(\mathbb{R}, Q_{\rm hum}) \cong \mathbb{R} \times TQ_{\rm hum}$, respectively, with local canonical variables $(t; x^i_{\rm rob}; \dot{x}^i_{\rm rob})$ and $(t; x^i_{\rm hum}; \dot{x}^i_{\rm hum})$, respectively. Its coordinate and velocity partial derivatives are respectively denoted by L_{x^i} and $L_{\dot{x}^i}$.

2.5 Local muscular mechanics

The right-hand side terms $\mathcal{F}_i(t, x, \dot{x})$ of (2) denote any type of external torques and forces, including excitation and contraction dynamics of muscular actuators and rotational dynamics of hybrid robot actuators, as well as (nonlinear) dissipative joint torques and forces and external stochastic perturbation torques and forces. In particular, we have [5–8]):

1. Synovial joint dynamics, giving the first stabilizing effect to the conservative skeleton dynamics, is described by the $(x, \dot{x})$-form of the Rayleigh–Van der Pol's dissipation function

$$R = \frac{1}{2}\sum_{i=1}^{n}(\dot{x}^i)^2\left[\alpha_i + \beta_i(x^i)^2\right],$$

where α_i and β_i denote dissipation parameters. Its partial derivatives give rise to the viscous-damping torques and forces in the joints

$$\mathcal{F}_i^{\rm joint} = \partial R/\partial \dot{x}^i,$$

which are linear in $\dot{x}^i$ and quadratic in x^i.

2. Muscular dynamics, giving the driving torques and forces $\mathcal{F}_i^{\rm muscle} = \mathcal{F}_i^{\rm muscle}(t, x, \dot{x})$ with $(i = 1, \ldots, n)$ for RHB, describes the internal excitation and contraction dynamics of equivalent muscular actuators [14].

(a) Excitation dynamics can be described by an impulse force–time relation

$$\begin{aligned} F_i^{\rm imp} &= F_i^0\left(1 - e^{-t/\tau_i}\right) && \text{if stimulation} > 0, \\ F_i^{\rm imp} &= F_i^0 e^{-t/\tau_i} && \text{if stimulation} = 0, \end{aligned}$$

where F_i^0 denote the maximal isometric muscular torques and forces, while τ_i denote the associated time

[5] In mechanics, we consider a pair of maps $f_1, f_2 : \mathbb{R} \to Q$ from the real line $\mathbb{R}$, representing the time t-axis, into a smooth nD configuration manifold Q. We say that the two maps $f_1 = f_1(t)$ and $f_2 = f_2(t)$ have the same k-jet $j^k_t f$ at a specified time instant $t_0 \in \mathbb{R}$, iff:

1. $f_1(t) = f_2(t)$ at $t_0 \in \mathbb{R}$; and also
2. The first k terms of their Taylor-series expansions around $t_0 \in \mathbb{R}$ are equal.

The set of all k-jets $j^k_t f : \mathbb{R} \to Q$ is the k-jet manifold $J^k(\mathbb{R}, Q)$. In particular, $J^1(\mathbb{R}, Q) \cong \mathbb{R} \times TQ$ (for technical details, see [8, 10]).

characteristics of particular muscular actuators. This relation represents a solution of the Wilkie's muscular active-state element equation [15]

$$\dot{\mu} + \gamma\mu = \gamma SA, \quad \mu(0) = 0,\ 0 < S < 1,$$

where $\mu = \mu(t)$ represents the active state of the muscle, γ denotes the element gain, A corresponds to the maximum tension the element can develop, and $S = S(r)$ is the 'desired' active state as a function of the motor unit stimulus rate r. This is the basis for the RHB force controller.

(b) Contraction dynamics has classically been described by the Hill's hyperbolic force–velocity relation [16]

$$F_i^{\text{Hill}} = \frac{(F_i^0 b_i - \delta_{ij} a_i \dot{x}^j)}{(\delta_{ij}\dot{x}^j + b_i)},$$

where a_i and b_i denote the Hill's parameters, corresponding to the energy dissipated during the contraction and the phosphagenic energy conversion rate, respectively, while δ_{ij} is the Kronecker's δ-tensor.

In this way, RHB describes the excitation/contraction dynamics for the ith equivalent muscle–joint actuator, using the simple impulse-hyperbolic product relation

$$\mathcal{F}_i^{\text{muscle}}(t, x, \dot{x}) = F_i^{\text{imp}} \times F_i^{\text{Hill}}.$$

Now, for the purpose of biomedical engineering and rehabilitation, RHB has developed the so-called hybrid rotational actuator. It includes, along with muscular and viscous forces, the D.C. motor drives, as used in robotics [5, 6, 17]:

$$\mathcal{F}_k^{\text{robo}} = i_k(t) - J_k\ddot{x}_k(t) - B_k\dot{x}_k(t),$$

with

$$l_k i_k(t) + R_k i_k(t) + C_k\dot{x}_k(t) = u_k(t),$$

where $k = 1, \ldots, n$, $i_k(t)$ and $u_k(t)$ denote currents and voltages in the rotors of the drives, R_k, l_k and C_k are resistances, inductances and capacitances in the rotors, respectively, while J_k and B_k correspond to inertia moments and viscous dampings of the drives, respectively.

Finally, to make the model more realistic, we need to add some stochastic torques and forces [1, 24]:

$$\mathcal{F}_i^{\text{stoch}} = B_{ij}\big[x^i(t), t\big]\, dW^j(t)$$

where $B_{ij}[x(t), t]$ represents continuous stochastic diffusion fluctuations, and $W^j(t)$ is an N-variable Wiener process (i.e. generalized Brownian motion), with $dW^j(t) = W^j(t + dt) - W^j(t)$ for $j = 1, \ldots, N$.

2.6 Hamiltonian biodynamics and reflex servo-control

The general form of Hamiltonian human/humanoid biodynamics on the corresponding symplectic cotangent bundles T^*Q_{rob} and T^*Q_{hum} of the configuration manifolds Q_{rob} and Q_{hum} (derived in [4, 6, 9]) is based on the affine Hamiltonian function $H_a : T^*Q \to \mathbb{R}$, in local canonical coordinates on T^*Q given as

$$H_a(x, p, u) = H_0(x, p) - H^j(x, p)u_j, \tag{3}$$

where $H_0(x, p)$ is the physical Hamiltonian (kinetic + potential energy) dependent on joint coordinates x^i and canonical momenta p^i, $H^j = H^j(x, p)$ ($j = 1, \ldots, m \le n$ are the coupling Hamiltonians corresponding to the system's active joints and $u_i = u_i(t, x, p)$ are (reflex) feedback controls). Using (3) we come to the affine Hamiltonian control HBE-system, in deterministic form:

$$\begin{aligned}
&\dot{x}^i = \partial_{p_i} H_0 - \partial_{p_i} H^j u_j + \partial_{p_i} R,\\
&\dot{p}_i = \mathcal{F}_i - \partial_{x^i} H_0 + \partial_{x^i} H^j u_j + \partial_{x^i} R,\\
&o^i = -\partial_{u_i} H_a = H^j,\\
&x^i(0) = x_0^i, \qquad p_i(0) = p_i^0,\\
&\quad (i = 1, \ldots, n;\ j = 1, \ldots,\ Q \le n)
\end{aligned} \tag{4}$$

(where $\partial_u \equiv \partial/\partial u$, $\mathcal{F}_i = \mathcal{F}_i(t, x, p)$, $H_0 = H_0(x, p)$, $H^j = H^j(x, p)$, $H_a = H_a(x, p, u)$, $R = R(x, p)$), as well as in the fuzzy-stochastic form [1, 24]:

$$\begin{aligned}
dq^i &= \big(\partial_{p_i} H_0(\sigma_\mu) - \partial_{p_i} H^j(\sigma_\mu)u_j + \partial_{p_i} R\big)\, dt,\\
dp_i &= B_{ij}\big[x^i(t), t\big]\, dW^j(t)\\
&\quad + \big(\bar{\mathcal{F}}_i - \partial_{x^i} H_0(\sigma_\mu)\\
&\quad + \partial_{x^i} H^j(\sigma_\mu)u_j + \partial_{x^i} R\big)\, dt,\\
d\bar{o}^i &= -\partial_{u_i} H_a(\sigma_\mu)\, dt = H^j(\sigma_\mu)\, dt,\\
x^i(0) &= \bar{x}_0^i, \qquad p_i(0) = \bar{p}_i^0.
\end{aligned} \tag{5}$$

In (4)–(5), $R = R(x, p)$ denotes the joint (nonlinear) dissipation function; o^i are affine system outputs (which can be different from joint coordinates); $\{\sigma\}_\mu$ (with $\mu \ge 1$) denote fuzzy sets of conservative parameters (segment lengths, masses and moments of inertia), dissipative joint dampings and actuator parameters (amplitudes and frequencies), while

the bar $(\bar{.})$ over a variable denotes the corresponding fuzzified variable; $B_{ij}[q^i(t),t]$ denote diffusion fluctuations and $W^j(t)$ are discontinuous jumps as the n-dimensional Wiener process.

In this way, the force HBE servo-controller is formulated as affine control Hamiltonian-systems (4)–(5), which resemble an autogenetic motor servo [18], acting on the spinal-reflex level of the human locomotion control. A voluntary contraction force F of human skeletal muscle is reflexily excited (positive feedback $+F^{-1}$) by the responses of its spindle receptors to stretch, and is reflexily inhibited (negative feedback $-F^{-1}$) by the responses of its Golgi tendon organs to contraction. Stretch and unloading reflexes are mediated by combined actions of several autogenetic neural pathways, forming the so-called 'motor servo.' The term 'autogenetic' means that the stimulus excites receptors located in the same muscle, which is the target of the reflex response. The most important of these muscle receptors are the primary and secondary endings in the muscle-spindles, which are sensitive to length change–positive length feedback $+F^{-1}$, and the Golgi tendon organs, which are sensitive to contractile force–negative force feedback $-F^{-1}$.

The gain G of the length feedback $+F^{-1}$ can be expressed as the positional stiffness (the ratio $G \approx S = dF/dx$ of the force-F change to the length-x change) of the muscle system. The greater the stiffness S, the less the muscle will be disturbed by a change in load. The autogenetic circuits $+F^{-1}$ and $-F^{-1}$ appear to function as servoregulatory loops that convey continuously graded amounts of excitation and inhibition to the large (alpha) skeletomotor neurons. Small (gamma) fusimotor neurons innervate the contractile poles of muscle spindles and function to modulate spindle-receptor discharge.

2.7 Cerebellum-like velocity and jerk control

Nonlinear velocity and jerk (time derivative of acceleration) servo-controllers [23], developed in HBE using the Lie-derivative formalism, resemble self-stabilizing and adaptive tracking action of the cerebellum [19]. By introducing the vector-fields f and g, given respectively by

$$f = (\partial_{p_i} H_0, -\partial_{q^i} H_0), \qquad g = \left(-\partial_{p_i} H^j, \partial_{q^i} H^j\right),$$

we obtain the affine controller in the standard nonlinear MIMO-system form (see [8, 20, 21]):

$$\dot{x}_i = f(x) + g(x)u_j. \tag{6}$$

Finally, using the Lie derivative formalism [10, 26][6] and applying the constant relative degree r to all HB joints, the control law for asymptotic tracking of the reference outputs $o_R^j = o_R^j(t)$ could be formulated as (generalized from [20])

$$u_j = \frac{\dot{o}_R^{(r)j} - L_f^{(r)} H^j + \sum_{s=1}^{r} c_{s-1}(o_R^{(s-1)j} - L_f^{(s-1)} H^j)}{L_g L_f^{(r-1)} H^j}, \tag{7}$$

where c_{s-1} are the coefficients of the linear differential equation of order r for the error function $e(t) = x^j(t) - o_R^j(t)$

$$e^{(r)} + c_{r-1}e^{(r-1)} + \cdots + c_1 e^{(1)} + c_0 e = 0.$$

The affine nonlinear MIMO control system (6) with the Lie-derivative control law (7) resembles the self-stabilizing and synergistic output tracking action of the human cerebellum [24, 26]. To make it adaptive (and thus more realistic), instead of the 'rigid' controller (7), we can use the adaptive Lie-derivative controller, as explained in the seminal paper on geometrical nonlinear control [22].

[6] Let $F(M)$ denote the set of all smooth (i.e., C^∞) real valued functions $f : M \to \mathbb{R}$ on a smooth manifold M, $V(M)$—the set of all smooth vector-fields on M, and $V^*(M)$—the set of all differential one-forms on M. Also, let the vector-field $\zeta \in V(M)$ be given with its local flow $\phi_t : M \to M$ such that at a point $x \in M$, $\frac{d}{dt}|_{t=0}\phi_t x = \zeta(x)$, and ϕ_t^* representing the pull-back by ϕ_t. The Lie derivative differential operator $\mathcal{L}_\zeta$ is defined:

(i) on a function $f \in F(M)$ as

$$\mathcal{L}_\zeta : F(M) \to F(M), \qquad \mathcal{L}_\zeta f = \frac{d}{dt}\left(\phi_t^* f\right)\big|_{t=0};$$

(ii) on a vector-field $\eta \in V(M)$ as

$$\mathcal{L}_\zeta : V(M) \to V(M), \qquad \mathcal{L}_\zeta \eta = \frac{d}{dt}\left(\phi_t^* \eta\right)\big|_{t=0} \equiv [\zeta, \eta],$$

the Lie bracket; and

(iii) on a one-form $\alpha \in V^*(M)$ as

$$\mathcal{L}_\zeta : V^*(M) \to V^*(M), \qquad \mathcal{L}_\zeta \alpha = \frac{d}{dt}\left(\phi_t^* \alpha\right)\big|_{t=0}.$$

In general, for any smooth tensor field $\mathbf{T}$ on M, the Lie derivative $\mathcal{L}_\zeta \mathbf{T}$ geometrically represents a directional derivative of $\mathbf{T}$ along the flow ϕ_t.

2.8 Cortical-like fuzzy-topological control

For the purpose of our cortical control, the dominant, rotational part of the human configuration manifold M^N, could be first reduced to an N-torus and then transformed to an N-cube ('hyper–joystick'), using the following topological techniques (see [8, 10, 26]).

Let S^1 denote the constrained unit circle in the complex plane, which is an Abelian Lie group. Firstly, we propose two reduction homeomorphisms, using the Cartesian product of the constrained $SO(2)$-groups:

$$SO(3) \approx SO(2) \times SO(2) \times SO(2) \quad \text{and}$$

$$SO(2) \approx S^1.$$

Next, let I^N be the unit cube $[0,1]^N$ in $\mathbb{R}^N$ and '$\sim$' an equivalence relation on $\mathbb{R}^N$ obtained by 'gluing' together the opposite sides of I^N, preserving their orientation. Therefore, M^N can be represented as the quotient space of $\mathbb{R}^N$ by the space of the integral lattice points in $\mathbb{R}^N$, i.e. an oriented and constrained N-dimensional torus T^N:

$$\mathbb{R}^N / Z^N \approx \prod_{i=1}^{N} S_i^1 \equiv \left\{ \left(q^i,\ i = 1, \ldots, N\right) : \mathrm{mod}\, 2\pi \right\} = T^N. \tag{8}$$

Its Euler–Poincaré characteristic is (by the De Rham theorem) both for the configuration manifold T^N and its momentum phase-space T^*T^N given by (see [10])

$$\chi\left(T^N, T^*T^N\right) = \sum_{p=1}^{N} (-1)^p b_p,$$

where b_p are the Betti numbers defined as

$$b^0 = 1,$$

$$b^1 = N, \qquad \ldots b^p = \binom{N}{p}, \qquad \ldots b^{N-1} = N,$$

$$b^N = 1 \quad (0 \le p \le N).$$

Conversely by 'ungluing' the configuration space we obtain the primary unit cube. Let '$\sim^*$' denote an equivalent decomposition or 'ungluing' relation. According to Tychonoff's product-topology theorem [8, 10], for every such quotient space there exists a 'selector' such that their quotient models are homeomorphic, that is, $T^N/\sim^* \approx A^N/\sim^*$. Therefore I_q^N represents a 'selector' for the configuration torus T^N and can be used as an N-directional '$\hat{q}$-command space' for the feedback control (FC). Any subset of degrees of freedom on the configuration torus T^N representing the joints included in HB has its simple, rectangular image in the rectified $\hat{q}$-command space selector I_q^N, and any joint angle q^i has its rectified image $\hat{q}^i$.

In the case of an end-effector, $\hat{q}^i$ reduces to the position vector in external-Cartesian coordinates z^r $(r = 1, \ldots, 3)$. If orientation of the end-effector can be neglected, this gives a topological solution to the standard inverse kinematics problem.

Analogously, all momenta $\hat{p}_i$ have their images as rectified momenta $\hat{p}_i$ in the $\hat{p}$-command space selector I_p^N. Therefore, the total momentum phase-space manifold T^*T^N obtains its 'cortical image' as the $\widehat{(q,\, p)}$-command space, a trivial $2N$-dimensional bundle $I_q^N \times I_p^N$.

Now, the simplest way to perform the feedback FC on the cortical $\widehat{(q,\, p)}$-command space $I_q^N \times I_p^N$, and also to mimic the cortical-like behavior, is to use the $2N$-dimensional fuzzy-logic controller, in much the same way as in the popular 'inverted pendulum' examples (see [27]).

We propose the fuzzy feedback-control map Ξ that maps all the rectified joint angles and momenta into the feedback-control one-forms

$$\Xi : \left(\hat{q}^i(t), \hat{p}_i(t)\right) \mapsto u_i(t, q, p), \tag{9}$$

so that their corresponding universes of discourse, $\hat{Q}^i = (\hat{q}^i_{\max} - \hat{q}^i_{\min})$, $\hat{P}_i = (\hat{p}_i^{\max} - \hat{p}_i^{\min})$ and $\hat{U}_i = (u_i^{\max} - u_i^{\min})$, respectively, are mapped as

$$\Xi : \prod_{i=1}^{N} \hat{Q}^i \times \prod_{i=1}^{N} \hat{P}_i \to \prod_{i=1}^{N} \hat{U}_i. \tag{10}$$

The $2N$-dimensional map Ξ (9)–(10) represents a fuzzy inference system, defined by (adapted from [28]):

1. Fuzzification of the crisp rectified and discretized angles, momenta and controls using Gaussian-bell membership functions

$$\mu_k(\chi) = \exp\left[-\frac{(\chi - m_k)^2}{2\sigma_k}\right] \quad (k = 1, 2, \ldots, 9),$$

where $\chi \in D$ is the common symbol for $\hat{q}^i$, $\hat{p}_i$ and $u_i(q, p)$ and D is the common symbol for $\hat{Q}^i$, $\hat{P}_i$ and $_i$; the mean values m_k of the nine

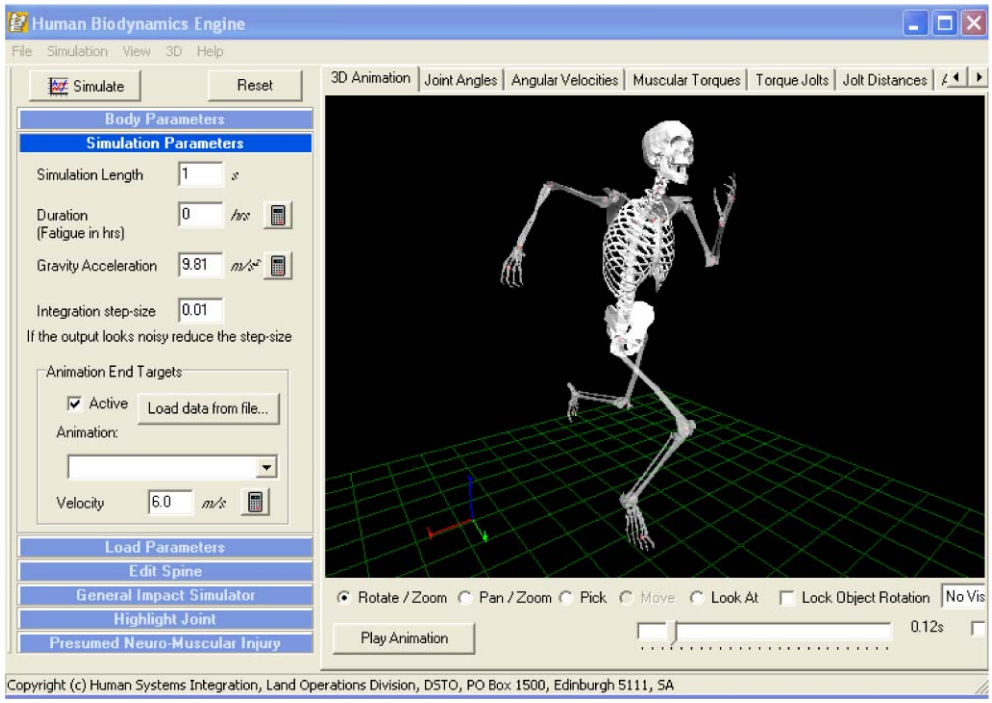

Fig. 5 Sample output from the Human Biodynamics Engine: running simulation with the speed of 6 m/s: a 3D animation view-port

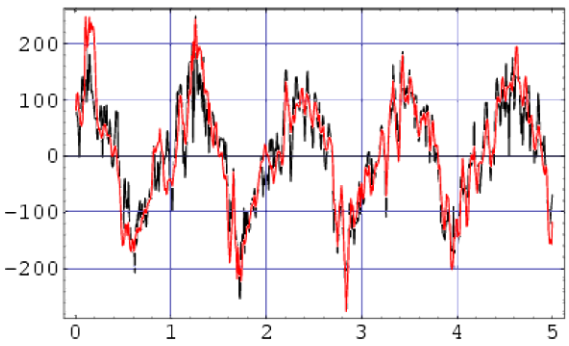

Fig. 6 Matching the 'Vicon' output with the 'HBE' output for the right-hip angular velocity around the dominant X-axis, while walking on a treadmill with a speed of 4 km/h

partitions of each universe of discourse D are defined as $m_k = \lambda_k D + \chi_{\min}$, with partition coefficients λ_k uniformly spanning the range of D, corresponding to the set of nine linguistic variables $L = \{NL, NB, NM, NS, ZE, PS, PM, PB, PL\}$; standard deviations are kept constant: $\sigma_k = D/9$. Using the linguistic vector L, the 9×9 FAM (fuzzy associative memory) matrix (a 'linguistic phase-plane') is heuristically defined for each human joint, in a symmetrical weighted form

$$\mu_{kl} = \varpi_{kl} \exp\{-50[\lambda_k + u(q, p)]^2\}$$

$$(k, l = 1, \ldots, 9)$$

with weights $\varpi_{kl} \in \{0.6, 0.6, 0.7, 0.7, 0.8, 0.8, 0.9, 0.9, 1.0\}$.

2. Mamdani inference is used on each FAM-matrix μ_{kl} for all human joints:
(i) $\mu(\hat{q}^i)$ and $\mu(\hat{p}_i)$ are combined inside the fuzzy IF–THEN rules using AND (Intersection, or Minimum) operator,

$$\mu_k[\bar{u}_i(q, p)] = \min_l\{\mu_{kl}(\hat{q}^i), \mu_{kl}(\hat{p}_i)\}.$$

(ii) The output sets from different IF–THEN rules are then combined using OR (Union, or Maximum) operator, to get the final output, fuzzy-covariant torques,

$$\mu[u_i(q, p)] = \max_k\{\mu_k[\bar{u}_i(q, p)]\}.$$

3. Defuzzification of the fuzzy controls $\mu[u_i(q,p)]$ with the 'center of gravity' method

$$u_i(q,p) = \frac{\int \mu[u_i(q,p)]\,du_i}{\int du_i},$$

to update the crisp feedback-control one-forms $u_i = u_i(t,q,p)$.

Now, it is easy to make this top-level controller adaptive, simply by weighting both the above fuzzy-rules and membership functions, by the use of any standard competitive neural network (see, e.g., [27]). Operationally, for the construction of the cortical $\widehat{(q,p)}$-command space $I_q^N \times I_p^N$ and the $2N$-dimensional feedback map Ξ (9)–(10), mimic the regulation of the motor conditioned reflexes by the motor cortex [19].

3 HBE simulation examples

The first version of the HBE simulator had the full human-like skeleton, driven by the generalized Hamiltonian dynamics (including muscular force–velocity and force–time curves) and two levels of reflex-like motor control (simulated using the Lie derivative formalism) [3, 6, 7]. It had 135 purely rotational DOF, strictly following Fig. 1. It was created for prediction and prevention of musculoskeletal injuries occurring in the joints, mostly spinal (intervertebral, see Fig. 4). Its performance looked kinematically realistic (see Fig. 5), while it was not possible to validate the driving torques. It included a small library of target movements which were followed by the HBE's Lie-derivative controllers with efficiency of about 90% (see Figs. 7 and 8).

The HBE also includes a generic crash simulator, based on the simplified road-vehicle impact simulator (see Fig. 9). While implementing the generic crash simulator, it became clear that purely rotational joint dynamics would not be sufficient for the realistic prediction of musculoskeletal injuries. Especially, to simulate the action of a Russian aircraft ejection-seat currently used by the American Space-shuttle, we needed, strictly following Fig. 2, to implement micro-translations in the intervertebral joints (see Figs. 10

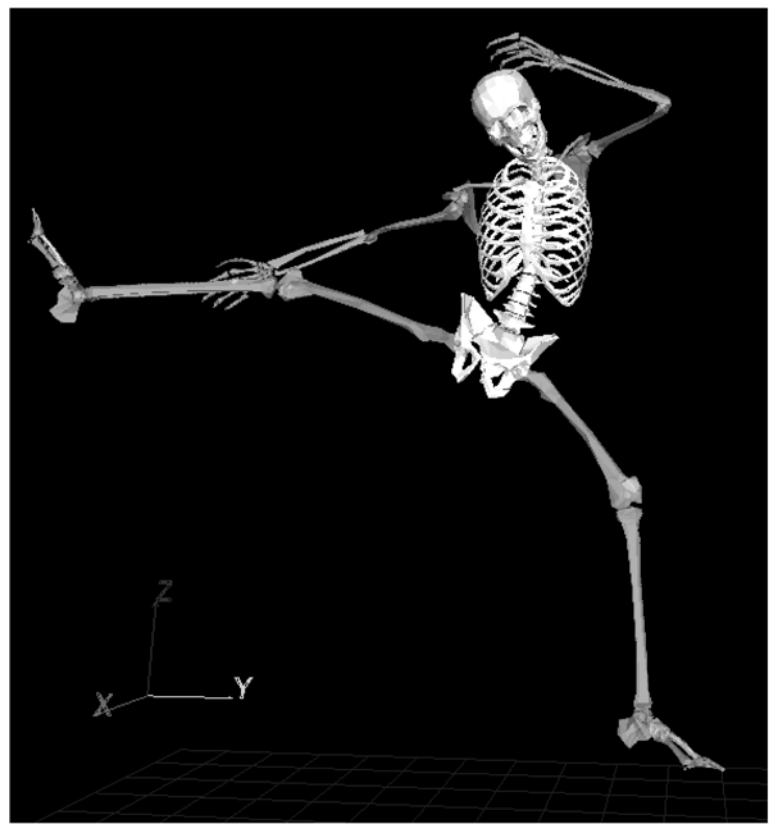

Fig. 7 The HBE simulating a jump-kick: a 3D viewer

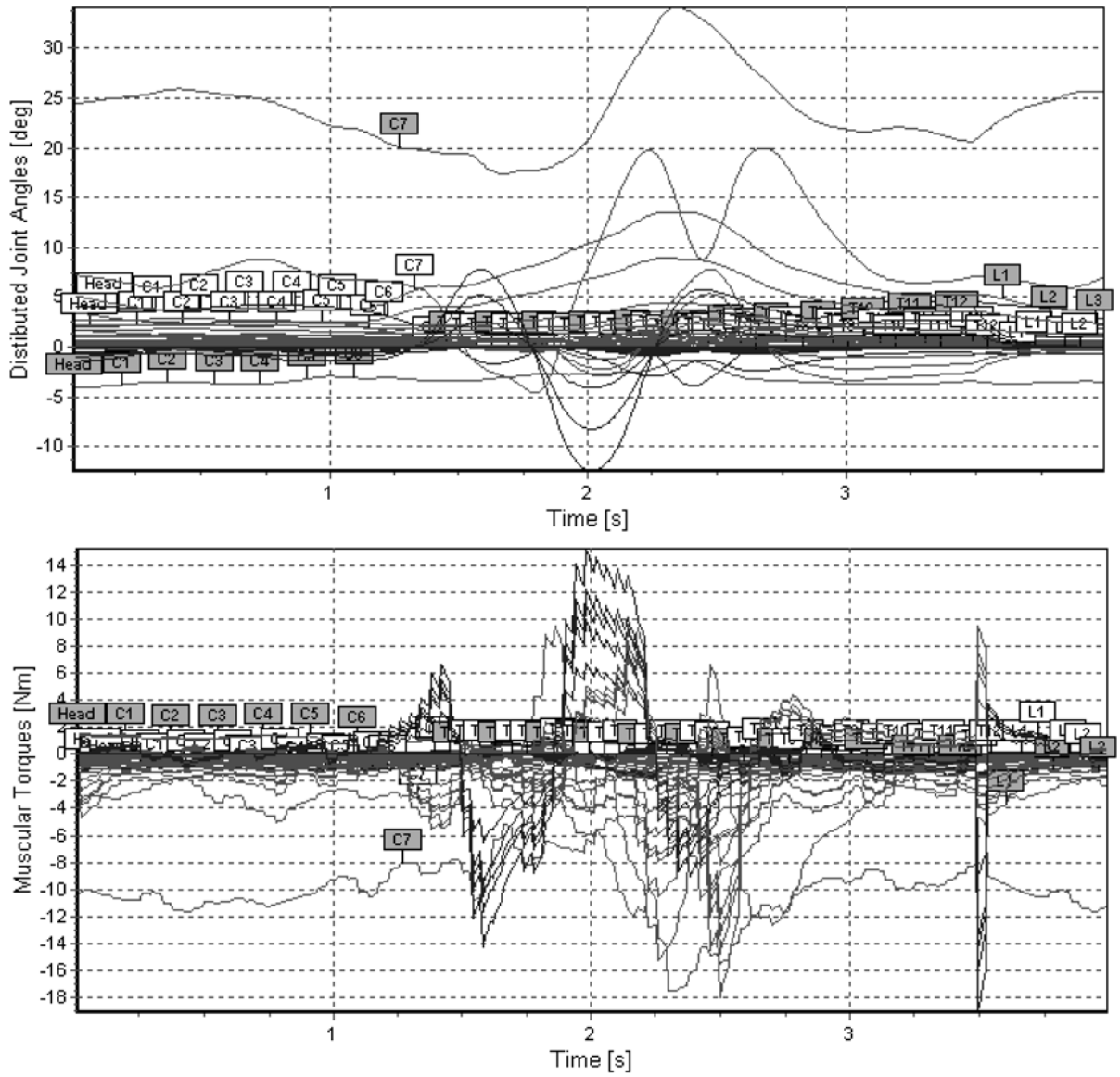

Fig. 8 The HBE simulating a jump-kick: calculating joint angles and muscular torques

and 11), as the seat provides the full body restraint and the ejection rockets, firing with 15 g for 0.15 s—can only compress the spine, without any bending at all.

Finally, the HBE includes the defense-specific land-mine crash simulator. It is calibrated on a hypothetical double-impact under the armor-protected military vehicle, including:

1. A land-mine blast of 350 g with a duration of 5 ms;
2. A 1 s pause when the hypothetical vehicle is in the air; and
3. The vehicle hard landing with an acceleration of 100 g and a duration of 1 s.

The HBE calculates full rotational and translational dynamics caused by the land-mine double-impact in extreme force/time scales (including both linear and angular displacements, velocities, forces and jolts in all human joints, see Fig. 12). The variations of the applied g-forces and durations of the two impacts can be simulated, to see the differences in their effects on the hypothetical passenger's body.

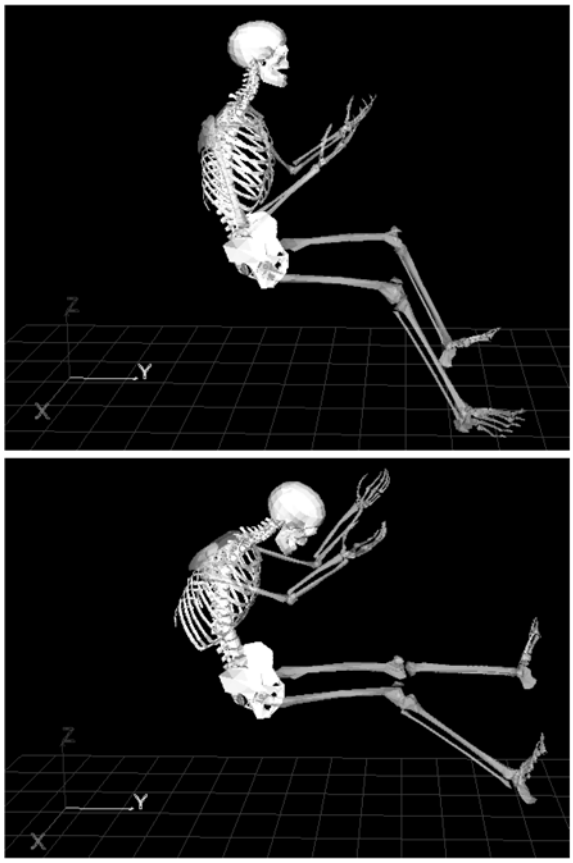

Fig. 9 The HBE simulating the frontal road-vehicle crash into the fixed wall with a speed of 70 km/h: before the impact (up) and 0.12 s after the impact

In this way a full rotational + translational biodynamics simulator has been created with 270 DOF in total (not representing separate fingers). The 'HBE-simulator' has been kinematically validated [29] against the standard biomechanical gait-analysis system 'Vicon' [30] (see Fig. 6).

4 Complexity of biodynamical behavior

4.1 Biodynamical 'entanglement'

From the standard engineering viewpoint, having two systems combined, in the case of biodynamics—biological and mechanical, as a single 'working machine'—we can expect that the total 'machine' complexity equals the sum of the two partial ones. For example, electrical circuitry has been a standard modeling framework in neurophysiology (A. Hodkgin and A. Huxley won a Nobel Prize for their circuit model of a single neuron, the celebrated HH-neuron [35]). Using the HH-approach for modeling human neuromuscular circuitry as electrical circuitry, we get an electromechanical model for our biomechanical system, in which the superposition of complexities is clearly valid.

On the other hand, in a recent research on dissipative quantum brain modeling, one of the most popular issues has been quantum entanglement[7] between the brain and its environment (see [31, 32]) where the brain–environment system has an entangled 'memory' state (identified with its ground state) that cannot be factorized into two single-mode states.[8] Similarly to this microscopic brain–environment entanglement, we conjecture the existence of a macroscopic neuro-mechanical entanglement between the operating modes of our neuromuscular controller and purely mechanical skeleton (see [40]).

In other words, we suggest that the diffeomorphism between the brain motion manifold (N-cube) and the body motion manifold M^N (which can be reduced to the constrained N-torus), described as the cortical motion control, can be considered a 'long-range correlation,' thus manifesting the 'biodynamical entanglement.'

4.2 Biodynamical self-assembly

In the framework of human motion dynamics, self-assembly represents adaptive motor control, i.e., physiological motor training performed by iteration of conditioned reflexes. For this, a combination of supervised and reinforcement training is commonly used, in which a number of (nonlinear) control parameters are iteratively adjusted similarly to the weights in neural networks, using either backpropagation-type or Hebbian-type learning, respectively (see, e.g., [27]). Every human motor skill is mastered using this general method. Once it is mastered, it becomes smooth and

[7] Entanglement is a term used in quantum theory to describe the way that particles of energy/matter can become correlated to predictably interact with each other regardless of how far apart they are; this is called a 'long–range correlation.'

[8] In the Vitiello–Pessa dissipative quantum brain model [31, 32], the evolution of a memory system was represented as a trajectory of given initial condition running over time-dependent states, each one minimizing the free energy functional.

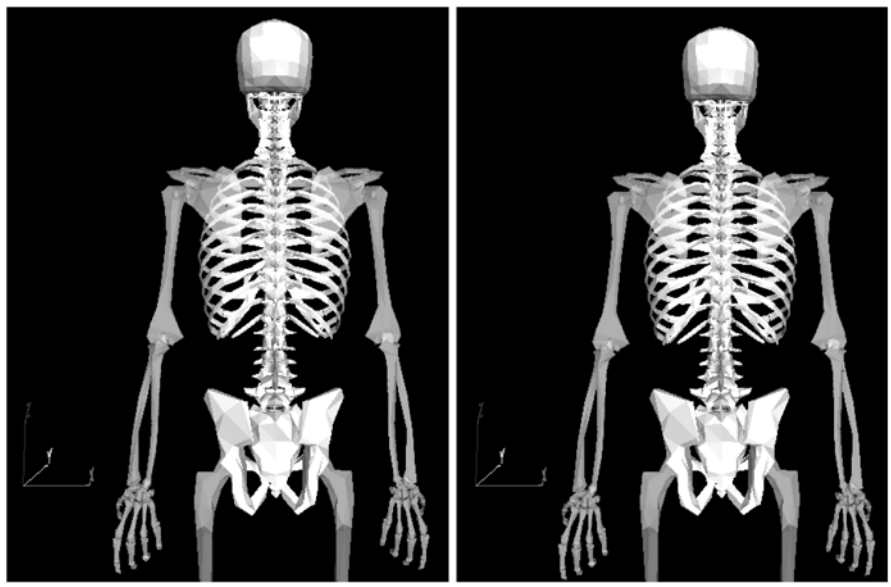

Fig. 10 The HBE simulating an effect of an aircraft pilot-seat ejection to human spine compression: before the seat ejection (*left*) and after ejection (*right*)

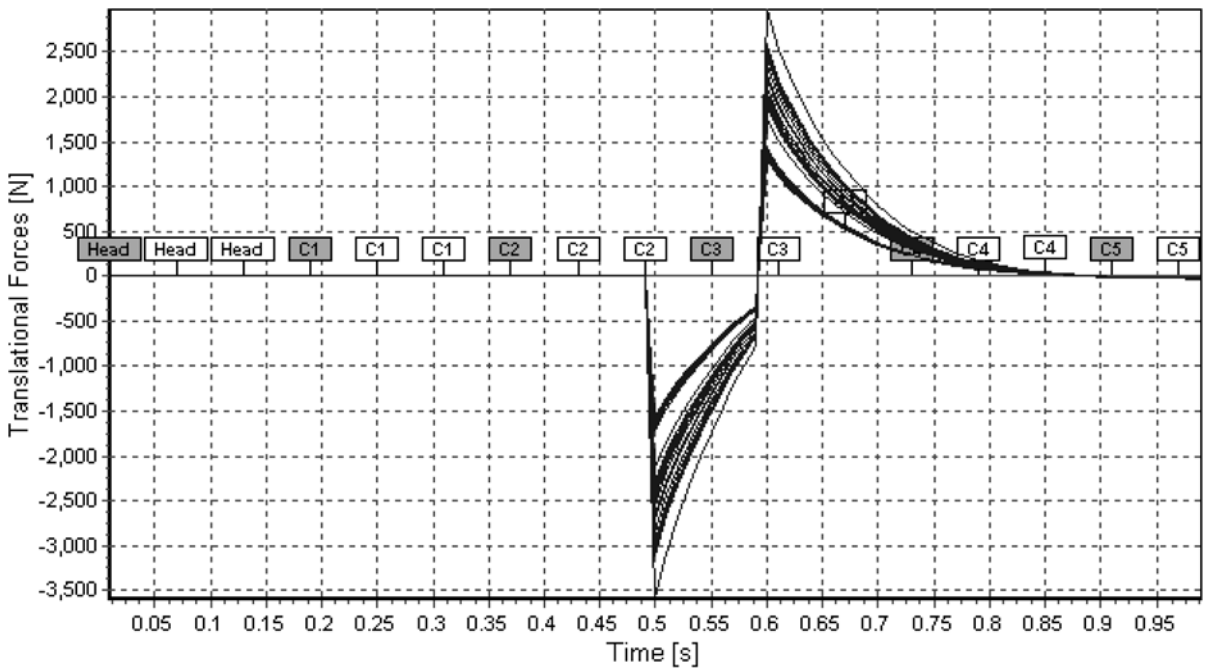

Fig. 11 The HBE calculating translational forces distributed along the spinal joints during the seat ejection

energy-efficient, in accordance with Bernstein's motor coordination and dexterity (see [33, 34]).

Therefore, biodynamical self-assembly clearly represents an 'evolution' in the parameter-space of human motion control. One might argue that such an evolution can be modeled using CA. However, this parameter-space, though being a dynamical and possibly even a contractible structure, is not an independent set of parameters—it is necessarily coupled to the mechanical skeleton configuration space, the plant to be controlled.

The system of 200 bones and 600 muscles can produce infinite number of different movements. In other words, the output-space dimension of a skilled human

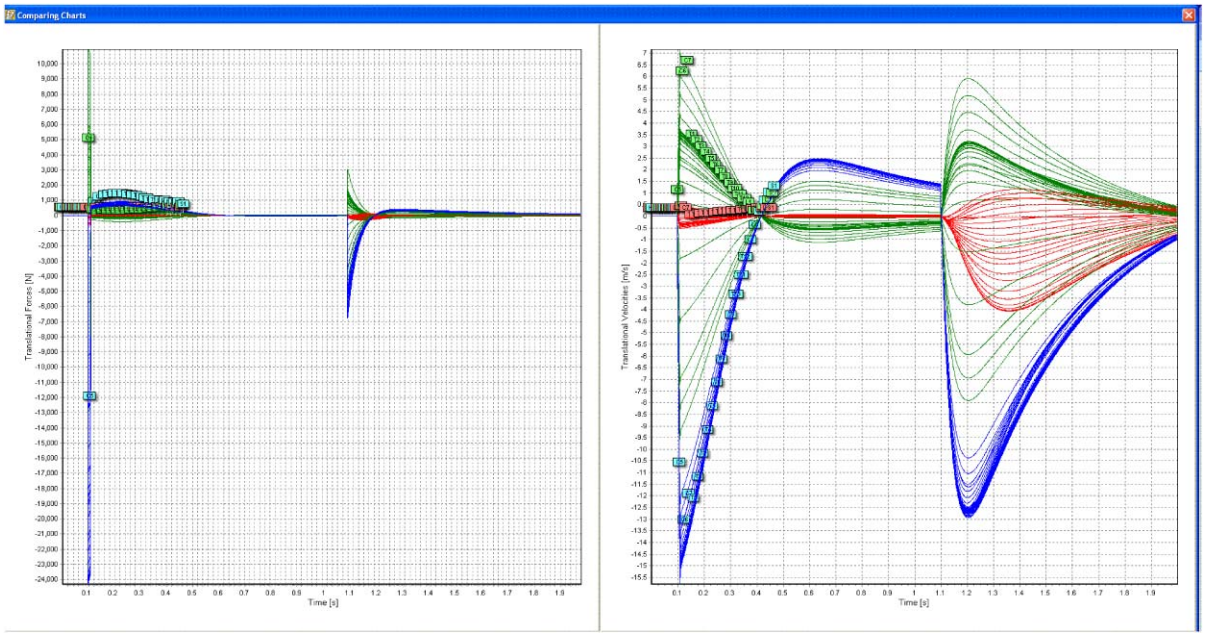

Fig. 12 The HBE simulating a double-impact effect of a land-mine blast under an armor-protected vehicle to a hypothetical passenger's body

motion dynamics equals infinity—there is no upper limit to the number of possible different human movements, starting with simple walk, run, jump, throw, play, etc. Even for the simplest motions, like walking, a child needs about 12 months to master it (and Honda robots took a decade to achieve this).

Furthermore, as human motion represents a simplest and yet well-defined example of a general human behavior, it is possible that other human behavioral and performance skills are mastered (i.e., self-assembled) in a similar way.

4.3 Biodynamical synchronization

The route to simplicity in biodynamics is synchronization. Both synchronization and phase-locking are ubiquitous in nature as well as in human brain (see [36–39]). Synchronization can occur in cyclic forms of human motion (e.g., walking, running, cycling, swimming), both externally, in the form of oscillatory dynamics, and internally, in the form of oscillatory cortical-control. This oscillatory synchronization, e.g., in walking dynamics, has three possible forms: in-phase, anti-phase, and out-of-phase. The underlying phase-locking properties determined by type of oscillator (e.g., periodic/chaotic, relaxation, bursting,[9] pulse-coupled, slowly connected, or connections with time delay) are involved in the cortical control system (motion planner). According to Izhikevich–Hoppensteadt work (ibid.), phase-locking is prominent in the brain: it frequently results in coherent activity of neurons and neuronal groups, as seen in recordings of local field potentials and EEG [25]. In essence,

[9] Periodic bursting behavior in neurons is a recurrent transition between a quiescent state and a state of repetitive firing. Three main types of neural bursters are: (i) parabolic bursting ('circle/circle'), (ii) square-wave bursting ('fold/homoclinic'), and (iii) elliptic bursting ('sub-Hopf/fold cycle'). Most burster models can be written in the singularly perturbed form:

$$x = f(x, y), \qquad y = \mu g(x, y),$$

where $x \in \mathbb{R}^m$ is a vector of fast variables responsible for repetitive firing (e.g., the membrane voltage and fast currents). The vector $y \in \mathbb{R}^k$ is a vector of slow variables that modulates the firing (e.g., slow (in)activation dynamics and changes in intracellular Ca^{2+} concentration). The small parameter $\mu \ll 1$ is a ratio of fast/slow timescales. The synchronization dynamics between bursters depends crucially on their spiking frequencies, i.e., the interactions are most effective when the presynaptic inter-spike frequency matches the frequency of postsynaptic oscillations. The synchronization dynamics between bursters in the cortical motion planner induces synchronization dynamics between upper and lower limbs in oscillatory motions.

the purpose of brain control of human motion is reduction of mechanical configuration space; brain achieves this through synchronization.

While cyclic movements indeed present a natural route to biodynamical synchronization, both on the dynamical and cortical-control level, the various forms of synchronized group behavior in sport (such as synchronized swimming, diving, acrobatics) or in military performance represent the imperfect products of hard training. The synchronized team performance is achievable, but the cost is a difficult long-term training and sacrifice of one's natural characteristics.

For more details on general complexity in human and robotic biomechanics, see [9].

5 Conclusion

We have presented various aspects of development of the Human Biodynamics Engine. The HBE geometry is based on anthropomorphic tree of Euclidean $SE(3)$-groups. Its dynamics was at first Lagrangian and later changed to Hamiltonian (dynamically equivalent, but superior for control). Its actuators are 'equivalent muscles,' following classical Hill–Hatze muscular mechanics. Its reflexes follow Houk's 'autogenetic' stretch-Golgi prescription. Its 'cerebellum' is modeled using Lie-derivative formalism. Its brain is fuzzy-topological. Its complexity shows biodynamical 'entanglement,' self-assembly and oscillatory synchronization. Its simulations demonstrate the necessity of micro-translations in the human joints, which cannot exist in robots. The main purpose for its development has been prediction of neuro-musculoskeletal injuries. For this purpose, the concept of rotational (soft) and translational (hard) jolts has been developed and implemented in HBE. The HBE-simulator is currently under the thorough validation process. Kinematic validation has mostly been completed, while for the validation of torques and forces, an adequate *in vivo* measurement technology is still lacking.

References

1. Ivancevic, V., Snoswell, M.: Fuzzy-stochastic functor machine for general humanoid–robot dynamics. IEEE Trans. Syst. Man Cybern., Part B **31**(3), 319–330 (2001)
2. Ivancevic, V.: Generalized Hamiltonian biodynamics and topology invariants of humanoid robots. Int. J. Math. Math. Sci. **31**(9), 555–565 (2002)
3. Ivancevic, V.: Symplectic rotational geometry in human biomechanics. SIAM Rev. **46**(3), 455–474 (2004)
4. Ivancevic, V., Beagley, N.: Brain-like functor control machine for general humanoid biodynamics. Int. J. Math. Math. Sci. **11**, 1759–1779 (2005)
5. Ivancevic, V.: Lie–Lagrangian model for realistic human bio-dynamics. Int. J. Hum. Robot. **3**(2), 205–218 (2006)
6. Ivancevic, V., Ivancevic, T.: Human-Like Biomechanics: A Unified Mathematical Approach to Human Biomechanics and Humanoid Robotics. Springer, Dordrecht (2006)
7. Ivancevic, V., Ivancevic, T.: Natural Biodynamics. World Scientific, Singapore (2006)
8. Ivancevic, V., Ivancevic, T.: Geometrical Dynamics of Complex Systems: A Unified Modelling Approach to Physics, Control, Biomechanics, Neurodynamics and Psycho-Socio-Economical Dynamics. Springer, Dordrecht (2006)
9. Ivancevic, V., Sharma, S.: Complexity in human biomechanics. Int. J. Hum. Robot. **5**(4), 679–698 (2008)
10. Ivancevic, V., Ivancevic, T.: Applied Differential Geometry: A Modern Introduction. World Scientific, Singapore (2007)
11. Ivancevic, V., Ivancevic, T.: Human versus humanoid biodynamics. Int. J. Hum. Robot. **5**(4), 699–713 (2008)
12. Marsden, J.E., Ratiu, T.S.: Introduction to Mechanics and Symmetry: A Basic Exposition of Classical Mechanical Systems, 2nd edn. Springer, New York (1999)
13. Park, J., Chung, W.-K.: Geometric integration on Euclidean group with application to articulated multibody systems. IEEE Trans. Rob. **21**(5), 850–863 (2005)
14. Hatze, H.: A general myocybernetic control model of skeletal muscle. Biol. Cybern. **28**, 143–157 (1978)
15. Wilkie, D.R.: The mechanical properties of muscle. Br. Med. Bull. **12**, 177–182 (1956)
16. Hill, A.V.: The heat of shortening and the dynamic constants of muscle. Proc. R. Soc. B **76**, 136–195 (1938)
17. Vukobratovic, M., Borovac, B., Surla, D., Stokic, D.: Biped Locomotion: Dynamics, Stability, Control, and Applications. Springer, Berlin (1990)
18. Houk, J.C.: Regulation of stiffness by skeletomotor reflexes. Annu. Rev. Physiol. **41**, 99–123 (1979)
19. Houk, J.C., Buckingham, J.T., Barto, A.G.: Models of the cerebellum and motor learning. Behav. Brain Sci. **19**(3), 368–383 (1996)
20. Isidori, A.: Nonlinear Control Systems, An Introduction, 2nd edn. Springer, Berlin (1989)
21. Nijmeijer, H., Van der Schaft, A.J.: Nonlinear Dynamical Control Systems. Springer, New York (1990)
22. Sastri, S.S., Isidori, A.: Adaptive control of linearizable systems. IEEE Trans. Autom. Control **34**(11), 1123–1131 (1989)
23. Ivancevic, V., Ivancevic, T.: High-Dimensional Chaotic and Attractor Systems. Springer, Berlin (2006)
24. Ivancevic, V., Ivancevic, T.: Neuro-Fuzzy Associative Machinery for Comprehensive Brain and Cognition Modelling. Springer, Berlin (2007)
25. Ivancevic, V., Ivancevic, T.: Computational Mind: A Complex Dynamics Perspective. Springer, Berlin (2007)
26. Ivancevic, V., Ivancevic, T.: Complex Dynamics: Advanced System Dynamics in Complex Variables. Springer, Dordrecht (2007)

27. Kosko, B.: Neural Networks and Fuzzy Systems, A Dynamical Systems Approach to Machine Intelligence. Prentice–Hall, New York (1992)
28. Ivancevic, T., Jain, L.C., Bottema, M.: A new two-feature GBAM-neurodynamical classifier for breast cancer diagnosis. In: Proc. KES'99. IEEE Press, New York (1999)
29. Ivancevic, V.: Kinematic Calibration and Validation of the Human Biodynamics Engine, Australian Def. Sci. Tec. Technical Report DSTO-TR-07 (in press)
30. Robertson, D.G.E., Caldwell, G.H., Hamill, J., Kamen, G., Whittlesey, S.N.: Research Methods in Biomechanics. Human Kinetics, Champaign (2004)
31. Pessa, E., Vitiello, G.: Quantum noise, entanglement and chaos in the quantum field theory of mind/brain states. Mind Matter **1**, 59–79 (2003)
32. Pessa, E., Vitiello, G.: Quantum noise induced entanglement and chaos in the dissipative quantum model of brain. Int. J. Mod. Phys. B **18**, 841–858 (2004)
33. Bernstein, N.A.: The Coordination and Regulation of Movements. Pergamon, Oxford (1967)
34. Bernstein, N.A.: On dexterity its development. In: Latash, M.L., Turvey, M.T. (eds.) Dexterity and its Development. Lawrence Erlbaum Associates, Mahwah (1996)
35. Hodgkin, A.L., Huxley, A.F.: A quantitative description of membrane current and application to conduction and excitation in nerve. J. Physiol. **117**, 500–544 (1952)
36. Hoppensteadt, F.C., Izhikevich, E.M.: Weakly Connected Neural Networks. Springer, New York (1997)
37. Hoppensteadt, F.C., Izhikevich, E.M.: Oscillatory neurocomputers with dynamic connectivity. Phys. Rev. Lett. **82**(14), 2983–2986 (1999)
38. Izhikevich, E.M.: Synchronization of elliptic bursters. SIAM Rev. **43**(2), 315–344 (2001)
39. Hoppensteadt, F.C., Izhikevich, E.M.: Canonical neural models. In: Arbib, M.A. (ed.) Brain Theory and Neural Networks, 2nd edn. MIT Press, Cambridge (2001)
40. Enoka, R.M.: Neuromechanics of Human Movement, 3rd edn. Human Kinetics, Champaign (2001)